Tanaka, M., Ozawa, T., Maurer, A., Cortese, J. D., & Fleischer, S. (1986) *Arch. Biochem. Biophys. 251*, 369–378.
Vidal, J. C., Guglielmucci, E. A., & Stoppani, A. O. M. (1977a) *Adv. Exp. Med. Biol. 83*, 203–217.
Vidal, J. C., Guglielmucci, E. A., & Stoppani, A. O. M. (1977b) *Mol. Cell. Biochem. 16*, 153–169.
Viratelle, O. M., & Seydoux, F. J. (1975) *J. Mol. Biol. 92*, 193–205.
Weber, G. (1972) *Biochemistry 11*, 864–878.
Weber, G. (1975) *Adv. Protein Chem. 29*, 1–83.
Whitehead, E. (1970) *Prog. Biophys. Mol. Biol. 21*, 321–397.
Wong, J. T.-F. (1975) in *Kinetic of Enzyme Mechanisms*, pp 123–140, Academic, London.
Wyman, J. (1964) *Adv. Protein Chem. 19*, 223–286.
Wyman, J. (1965) *J. Mol. Biol. 11*, 631–644.
Wyman, J. (1967) *J. Am. Chem. Soc. 89*, 2202–2218.
Wyman, J. (1968) *Q. Rev. Biophys. 1*, 35–80.
Wyman, J., & Phillipson, P. E. (1974) *Proc. Natl. Acad. Sci. U.S.A. 71*, 3431–3434.

Hydration of Carbon Dioxide by Carbonic Anhydrase: Internal Proton Transfer of Zn^{2+}-Bound HCO_3^- †

Jiin-Yun Liang and William N. Lipscomb*
Gibbs Chemical Laboratories, Department of Chemistry, Harvard University, Cambridge, Massachusetts 02138
Received January 2, 1987; Revised Manuscript Received March 31, 1987

ABSTRACT: Proton transfer within HCO_3^- has been examined under various conditions through molecular orbital methods: partial retention of diatomic differential overlap and 4-31G self-consistent field programs. These conditions include the absence or presence of Zn^{2+}, $Zn^{2+}(NH_3)_3$, or a water ligand on Zn^{2+}. In addition, 4-31G+ and some MP2/4-31G** results are obtained. The use of Be^{2+} to simulate Zn^{2+} reproduces reaction pathways and energy barriers, except for marginal cases. The barrier of 35.6 kcal/mol for direct internal proton transfer is reduced to 3.5 kcal/mol when one water molecule, not bound to Zn^{2+}, is included for proton relay and to 1.4 kcal/mol when two such water molecules are included. In the enzyme, either Thr-199 or solvent molecules could perform this relay function. Our results favor this facilitated proton transfer over a mechanism in which Zn^{2+}-bound OH^- attacks CO_2, a bidentate intermediate forms, and the OH moiety of the resulting HCO_3^- dissociates from Zn^{2+}, thus leaving one of the oxygens of the original CO_2 as a ligand to Zn^{2+}.

Carbonic anhydrase is a zinc metalloenzyme that catalyzes the reversible hydration of CO_2 to bicarbonate ion and a proton. In human carbonic anhydrase II (HCA II) the maximal turnover rate is 10^6 s^{-1} at 25 °C. It is now widely accepted that initial nucleophilic attack occurs by a Zn^{2+}-bound hydroxide ion and that subsequent proton transfer is catalyzed by a non Zn^{2+}-liganded histidine and by buffer in HCA II (Lindskog, 1983; Lindskog et al., 1984; Pocker & Sarkanen, 1978; Prince, 1979; Coleman et al., 1980; Lipscomb, 1983). A plausible sequence (Figure 1) for the hydration reaction is the following: (1) binding of CO_2 near Zn^{2+}; (2) conversion of CO_2 to HCO_3^- by nucleophilic attack of Zn^{2+}-bound OH^- on C of CO_2; (3) internal proton transfer of Zn^{2+}-bound HCO_3^-; (4) binding of H_2O to Zn^{2+} and ionization of this Zn^{2+}-bound H_2O to facilitate release of HCO_3^-; and (5) the coordinated transfer of H^+ from Zn^{2+}-bound H_2O to a proton-transfer group (His-64 in HCA II), then to buffer, and then to solvent. Not least among the ambiguities are five coordinated Zn^{2+} species, which can be formulated as intermediates in Figure 1. Examples are the transient binding of one oxygen of CO_2 to Zn^{2+} (step 2), the binding of both an OH and a terminal O of HCO_3^- to Zn^{2+} (step 3), and the binding of both H_2O and HCO_3^- (step 4).

In this paper we examine the proton transfer of step 3. The need for this transfer can be seen by comparing the forward reaction, in which the attack of Zn^{2+}-bound OH^- on CO_2 leaves the proton on a Zn^{2+}-bound oxygen, with the reverse reaction in which HCO_3^- may be expected to bind with an unprotonated oxygen to Zn^{2+} (Figure 1). Microscopic reversibility (Fersht, 1977) thus requires the proton transfer of step 3. In alkyl carbonate anions (RCO_3^-), which are known to bind as well as do alkyl carboxylates (RCO_2^-) to the enzyme, no substrate activity occurs (Pocker & Deits, 1983). Here, the proton is replaced by an alkyl group. If steric and pK_a factors are not problems, these results (Pocker & Deits, 1983) may support the proton transfer, which we now examine.

Methods

(*1*) *Basis Sets.* Partial retention of diatomic differential overlap (PRDDO) (Halgren & Lipscomb, 1973; Marynick & Lipscomb, 1982) uses an orthogonalized basis. It is a close approximation to the self-consistent field (SCF) MO calculations at the minimum basis set level. One-, two-, and three-center integrals of the form $(\chi_{ia}\chi_{jb}|\chi_{kc}^2)$ are retained, where χ_{ia} is a symmetrically orthogonalized AO mainly centered on the atom a. Also retained are one- and two-center exchange integrals of the form $(\chi_{ia}\chi_{ja}|\chi_{ia}\chi_{ja})$ and $(\chi_{ia}\chi_{ja}|\chi_{ia}\chi_{jb})$. Problems of rotational invariance are avoided by choice of local axes that are unique in anisotropic environments. Retention of $\sim N^3$ integrals in PRDDO is shown to simulate efficiently the STO-3G SCF results (Halgren et al., 1978; Scheiner et al., 1976). We also employ the Gaussian 82 program using the 4-31G basis of Pople (Ditchfield et al., 1971), and the 4-31G+ basis (Clark et al., 1983) obtained by adding sp type diffuse orbitals (with exponents 0.04 for C and 0.068 for O) on the heavy atoms in 4-31G. A limited number of 4-31G**

† This research was supported by the National Science Foundation (CHE-85-15347 and PCM-77-11398) and the National Institutes of Health (GM06920).

0006-2960/87/0426-5293$01.50/0

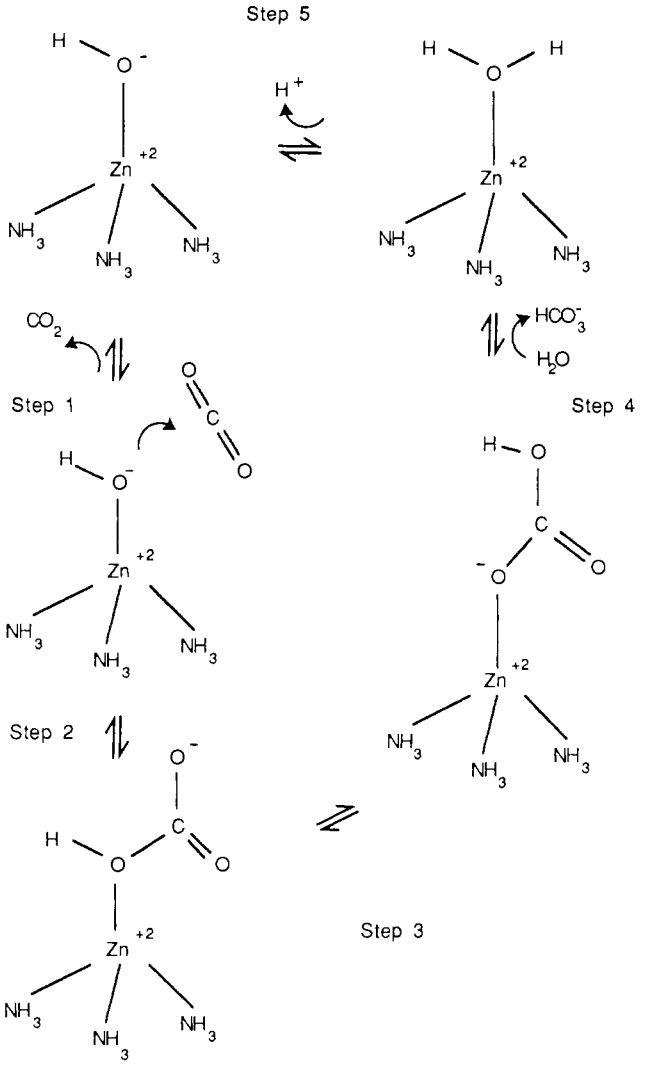

FIGURE 1: Enzymic reaction of CO_2 hydration consists of the following steps: (1) binding of CO_2 near Zn^{2+}; (2) conversion of CO_2 to HCO_3^- by nucleophilic attack of Zn^{2+}-bound OH^- on C of CO_2; (3) internal proton transfer of Zn^{2+}-bound HCO_3^-; (4) binding of H_2O to Zn^{2+} and ionization of this Zn^{2+}-bound H_2O to facilitate release of HCO_3^-; and (5) the coordinated transfer of H^+ from Zn^{2+}-bound H_2O to a proton-transfer group (His-64 in HCA II) and then to buffer and then to solvent. Note that the NH_3 molecules used here simulate the three imidazole ligands of Zn^{2+} from His-94, His-96, and His-119.

(Hariharan & Pople, 1973) calculations are also included, and correlation corrections are obtained by Møller–Plesset perturbations (Møller & Plesset, 1934) of the 4-31G** wave function to second order (MP2).

(*2*) *Reaction Pathways and Energy Barriers.* For all reactions studied here (Figure 2), the O_1–C–H_1 angle is the only reaction coordinate. In order to obtain the reaction paths, we first trace the energy curves along the reaction coordinate using the PRDDO method. On these energy curves we then locate the stationary points: the reactants, the transition states, and the products. Further geometry optimizations at the 4-31G level are carried out around these stationary points. During the geometry optimizations, planar geometries are assumed for complexes HCO_3^-, $Zn^{2+}(HCO_3^-)$, $Be^{2+}(HCO_3^-)$, Be^{2+}-$(HCO_3^-)H_2O$, $HCO_3^-(H_2O)$, and $HCO_3^-(H_2O)_2$ (Figure 2). In reaction 4, $(NH_3)_3$ simulates the imidazole groups of His-94, His-96, and His-119 in the active site of carbonic anhydrase. This substitution of NH_3 for imidazole is supported by the previous finding that NH_3 and imidazole transfer a similar amount of charge to Zn^{2+} (Pullman & Demoulin, 1979). Given that N–Be–N = 109.49° and that both NH_3 and $Zn^{2+}(NH_3)_3$ have C_3 symmetry, the structure of the $Zn^{2+}(NH_3)_3$ complex of reaction 4 is optimized. The results are Zn–N = 2.021 Å, N–H = 1.025 Å, and H–N–Zn = 112.8°. Under the same optimization condition, we obtain for the $Be^{2+}(NH_3)_3$ complex of reaction 4′ H–N–Be = 104.2°, N–H = 1.03 Å, and N–Be = 1.76 Å. In reaction 4a, the N–Zn–O angle of the $Zn^{2+}(NH_3)_3$ complex optimizes to 95.6°, and the other geometry parameters are N–Zn–O = 95.6°, H–N–Zn = 112.9°, N–H = 1.025 Å, and N–Zn = 2.02 Å. These optimized $Zn^{2+}(NH_3)_3$ and $Be^{2+}(NH_3)_3$ structures are held constant in the subsequent studies of the internal proton transfer of HCO_3^-.

Results

Table I contains optimized molecular geometries and Table II the energy barriers for all reactions studied here. Mulliken's population analyses (Mulliken, 1955) of atomic charges and bond orders are given in Tables A and B of the supplementary material for the PRDDO and the 4-31G results, respectively. In the following text, the forward reactions proceed from left to right in Figure 2 and the reverse reactions from right to left.

Reaction 1. Reaction 1 is the normal gas-phase reaction of internal proton transfer of HCO_3^- (Figure 2). During the forward proton transfer from reactant to transition state, loss of the negative charge on atom H_1 of 0.09 is largely compensated by the total gain of negative charge including both atoms O_1 and O_2 of 0.16 (Tables A and B, supplementary material). In the four-membered (C–O_1–H_1–O_2) proton-transfer ring, the decrease in the bond order of C–O_1 by 0.17 and of O_2–H_1 by 0.22 is balanced by the increase in the bond order of O_2–H_1 by 0.25 and of C–O_2 by 0.11 (Tables A and B, supplementary material). Of course, both the forward and reverse reactions have the same barrier: 35.6, 41.2, and 34.0 kcal/mol in PRDDO, 4-31G, and 6-31G**, respectively. When 4-31G+, 4-31G**, and 4-31G**/MP2 are applied at the 4-31G optimized geometries, the barriers are 43.3, 35.4, and 22.7 kcal/mol, respectively (Table II).

Reaction 2. In the reactant of reaction 2, Zn^{2+} is coordinated to O_1 of HCO_3^- (Figure 2). This addition of Zn^{2+} results in the transfer of 0.9 electrons from HCO_3^- to Zn^{2+} (Table A, supplementary material). The electron withdrawal from HCO_3^- and the electrostatic repulsion between the positive charges on Zn^{2+} (1.1) and those on the transferring proton (0.3) may lead to destabilization of the proton transfer. This destabilization is balanced at the transition state by partial bidentate coordination of HCO_3^- to Zn^{2+} (Table I). The barrier for the forward reaction is 30.5 kcal/mol (Table II). In the product, further stabilization is obtained by the coordination of both O_1 and O_3 of HCO_3^- to Zn^{2+}. This stabilizing effect for the product is larger than that for the transition state. A large reverse barrier, 69.4 kcal/mol, is obtained (PRDDO).

Reaction 3. During the internal proton transfer of reaction 3, both O_1 and O_3 of HCO_3^- are coordinated to Zn^{2+} (Figure 2). The bond order of Zn–O_1 in the reactant of reaction 2 (0.54) is replaced in reaction 3 by the sum of bond orders of Zn–O_1 (0.29) and Zn–O_3 (0.27) (Table A, supplementary material). The bond length of C–O_1 changes in the forward proton transfer from 1.32 Å in the reactant to 1.36 Å at the transition state and then to 1.48 Å in the product (Table I). The product of reaction 3 is identical with that of reaction 2, and the barriers for the forward and the reverse reactions are 67.5 and 59.6 kcal/mol, respectively (Table II).

Reaction 4. In reaction 4, three NH_3 molecules (denoted as $(NH_3)_3$) are coordinated to Zn^{2+} to simulate the three imidazole ligands of Zn^{2+} (His-94, His-96, and His-119) in

Table I: Molecular Geometries for Reactants, Transition States, and Products of Reactions Shown in Figure 2[a]

state	bond lengths (Å)									bond angles (deg)
	$C-O_1$	$C-O_2$	$C-O_3$	O_1-H_1	O_2-H_1	$Be-O_1$	$Be-O_3$	H_2-O_4	O_4-H_1	O_1-C-O_2
4-31G Results										
1-r	1.2524	1.4257	1.2353	2.2275	0.9514					113.4
1-ts	1.3439	1.3439	1.2217	1.2687	1.2687					101.1
2′-r	1.3997	1.3079	1.1821	2.3604	0.9535	1.3711	3.1997			112.5
2′-ts	2.1681	1.2305	1.1231	1.7170	1.0030	1.3491	2.9172			81.4
2′-p	4.0864	1.1870	1.1874	0.9374	6.1482	1.3500	1.5490			179.7
2′-p[b]	2.1942	1.1662	1.1533	1.1076	1.7492	1.3525	3.1241			88.3
3′-r	1.3163	1.2586	1.3039	2.5517	0.9629	1.5874	1.5784			126.9
3′-ts	1.4060	1.2173	1.2924	1.3266	1.4152	1.5890	1.5881			106.7
3′-p[h]										
3′-p[b]	1.4444	1.1656	1.3337	0.9258	2.1995	1.6434	1.4763			122.2
6-r	1.2700	1.4017	1.2258	1.6464[c]	0.9538			0.9839	2.3128	114.3
6-ts	1.3330	1.3330	1.2173	1.0282[c]	1.0282			1.4604	1.4604	114.4
PRDDO Results										
1-r	1.2586	1.4463	1.2498	2.2258	0.9953					113.6
1-ts	1.3578	1.3578	1.2332	1.2371	1.2371					98.0
2-r	1.3746	1.3670	1.2240	2.2937	0.9880	1.6841[d]	3.7288[d]			113.6
2-ts	1.3625	1.3771	1.2523	1.2933	1.2533	1.8721[d]	2.4005[d]			93.2
2-p	1.4757	1.2073	1.3169	0.9653	2.5691	1.9545[d]	1.9142[d]			119.6
2′-r	1.4143	1.3416	1.2121	2.3067	0.9850	1.3147	3.4044			113.5
2′-ts	1.8657	1.2731	1.1698	1.2708	1.1215	1.3382	3.5289			84.1
2′-p	2.4813	1.2109	1.1787	1.0105	1.4758	1.2925	3.5907			71.8
2a-r	1.3990	1.3372	1.2190	2.2069	1.0033	1.6	2.7953			114.9
2a-ts	1.9896	1.2765	1.1752	1.2949	1.1092	1.6	3.3894			79.9
2a-p	3.0635	1.2065	1.1784	1.0114	1.4289	1.6	2.4445			48.6
2b-r	1.3795	1.3545	1.2256	2.2807	0.9933	1.8	2.9421			114.0
2b-ts	1.5738	1.3260	1.1962	1.0938	1.3519	1.8	3.1387			86.4
2b-p	1.4124	1.1044	1.3533	0.9919	2.4486	1.8	2.4445			124.6
2c-r	1.3944	1.3689	1.2211	2.3149	0.9817	1.8	3.9130			114.4
2c-ts	2.2042	1.2609	1.1653	1.6492	1.0753	1.8	4.3462			84.5
2c-p	3.1494	1.2055	1.1779	1.0299	1.4293	1.8	5.4053			47.2
3-r	1.3217	1.3170	1.3066	2.3859	1.0147	1.8943[d]	2.0525[d]			121.0
3-ts	1.3604	1.3125	1.2793	1.2105	1.3514	1.8777[d]	2.1050[d]			96.5
3-p[h]										
3′-r	1.3329	1.2923	1.3311	2.5423	1.0008	1.5825	1.3311			127.9
3′-ts	1.4055	1.2569	1.3272	1.2321	1.3101	1.5590	1.6122			100.0
3′-p	1.5013	1.1785	1.3453	0.9797	2.7093	1.5465	1.5339			123.0
4-r	1.3155	1.4035	1.2505	2.5174	1.0866	1.8262[d]	2.6938[d]			112.1
4-ts	1.4041	1.2530	1.2700	1.2995	1.7749	1.8572[d]	2.4238[d]			112.3
4-p	1.4941	1.2211	1.2648	0.9844	2.3757	1.8848[d]	2.5539[d]			114.2
4a-r	1.3260	1.3686	1.2374	2.2166	0.9874	1.8719[d]	2.9474[d]			114.0
4a-ts	1.5235	1.2785	1.2236	1.1133	1.5436	1.8996[d]	2.8867[d]			100.6
4a-p	1.5011	1.2232	1.2592	0.9897	2.3407	1.8884[d]	2.5756[d]			113.5
4′-r	1.3286	1.3768	1.2258	2.2339	0.9861	1.4488	2.8845			113.6
4′-ts	1.5283	1.2796	1.2236	1.1042	1.5404	1.4867	2.7878			99.8
4′-p	1.5472	1.2118	1.2447	0.9644	2.2439	1.5216	2.4534			110.7
5a-r	1.3222	1.3280	1.2615	2.3208	0.9950	1.4823	1.6785[d]	1.0	1.3112	119.5
5a-ts	1.3193	1.2947	1.2680	1.6235	1.2355	1.5046	1.6403[e]	1.1657	1.1838	117.8
5a-p	1.5333	1.1976	1.2845	0.9937	2.0591	1.6034	1.5536[e]	1.1	1.1594	109.8
5b-r	1.3065	1.3393	1.2426	2.2914	0.9883	1.4586	1.5082[e]	1.1456	1.2384	118.4
5b-ts	1.4448	1.2292	1.2878	1.1353	1.4832	1.5231	1.4226[e]	1.4250	1.0533	99.2
5b-p	1.5208	1.2060	1.2815	0.9836	2.1046	1.5164	1.4289[e]	1.1500	1.1213	108.7
5c-r	1.3162	1.3158	1.2856	2.3214	0.9940	1.4581	1.4054[e]	1.3513	1.0705	119.7
5c-ts	1.5123	1.2278	1.2652	1.1822	1.4478	1.3920	1.4259[e]	1.1659	1.1452	96.8
5c-p	1.6670	1.1997	1.2577	0.9818	2.1319	1.4426	1.4277[e]	1.1847	1.1341	102.2
6-r	1.3019	1.4062	1.2450	1.3048[c]	0.9925			1.0699	1.5939	115.7
6-ts	1.3360	1.3362	1.2626	1.0633[c]	1.0633			1.2361	1.2361	119.2
6a-r	1.4457	1.2795	1.2449	1.7339[c]	1.0000	1.5000	2.6399	0.9785	1.2934	116.5
6a-ts	1.4801	1.2472	1.2657	1.2000[c]	1.2255	1.5000	2.5687	1.0978	1.0934	112.8
6a-p	1.5096	1.2311	1.2723	1.1881[c]	1.4432	1.5000	2.5318	1.1316	1.0277	113.5
7-r	1.2598	1.4462	1.2494	1.3956	0.9951	1.5262[f]	1.0299[g]	0.9950	1.7861	114.0
7-ts	1.3601	1.3601	1.2449	1.0506	1.0506	1.1670[f]	1.4706[g]	1.1670	1.4706	115.7

[a] Each state listed here is designated by the reaction number and the corresponding stage of reaction. Three stages for each reaction are the reactant (r), the transition state (ts), and the product (p). All reactions are shown in Figure 2. Reactions 2, 3, 4, and 4a involve the Zn^{2+} ion. Reactions 2′, 2a, 2b, 2c, 3′, 4′, 5a, 5b, 5c, and 6a involve the Be^{2+} ion. Reactions 6 and 7 are one-water and two-water proton relay, respectively. Molecular geometries are optimized with the PRDDO method and in some cases with the SCF MO method at the 4-31G level. Reactions involving the transition-metal Zn^{2+} are studied only at the PRDDO level. In the geometry optimization of reaction 2b, geometry constraints are applied; they are $Be^{2+}-O_1 = 1.6$ Å, $Be-O_1-C = 120.0°$, and the dihedral angle of $Be-O_1-C-O_3 = 0.0°$. In reaction 2c, the constraints are $Be-O_1 = 1.8$ Å, $Be-O_1-C = 120.0°$, and the dihedral angle of $Be-O_1-C-O_3 = 0.0°$. In reaction 2d, $Be-O_1 = 1.8$ Å, $Be-O_1-C = 120.0°$, and the dihedral angle of $Be-O_1-C-O_3 = 180.0°$. In reactions 5a, 5b, and 5c, O_1-Be-O_4 is 80°, 100°, and 120°, respectively. In reaction 6a, $Be-O_1 = 1.5$ Å and $Be-O_1-C = 120.0°$. [b] The optimized geometry is obtained at the 4-31G level with $H_1-C-O_1 = 30°$ in the product. [c] Bond length of O_1-H_2. [d] $Be-O_1$ and $Be-O_3$ are replaced by $Zn-O_1$ and $Zn-O_3$, respectively. [e] Bond length of $Be-O_4$. [f] Bond length of O_5-H_2. [g] Bond length of O_5-H_3. [h] Same as for 2′-p.

Reaction 1. (PRDDO and 4-31G)

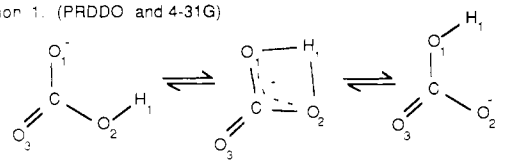

Reaction 2. (PRDDO)

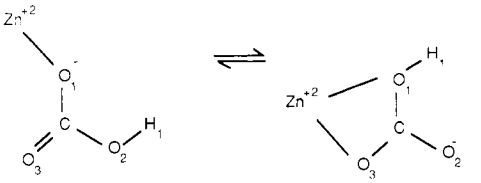

Reaction 3. (PRDDO)

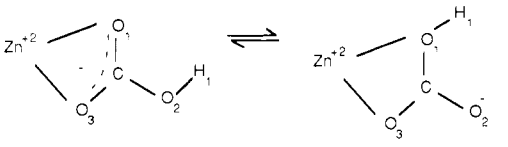

Reaction 4 and 4a (PRDDO)

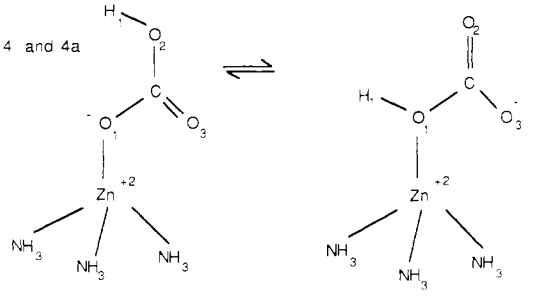

Reaction 2'. (PRDDO)

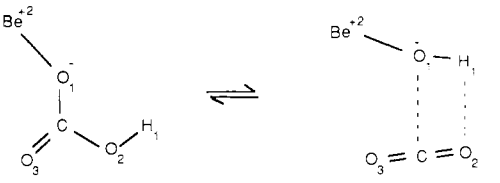

Reaction 2'. (4-31G)

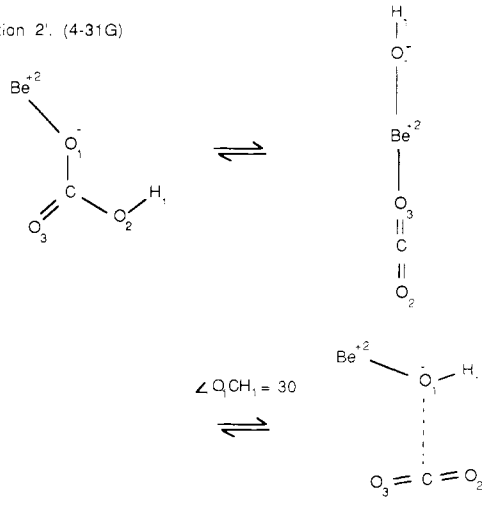

Reaction 3'. (PRDDO)

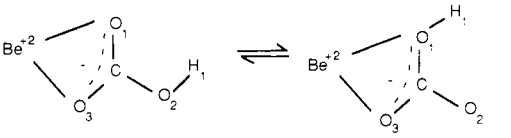

Reaction 3'. (4-31G)

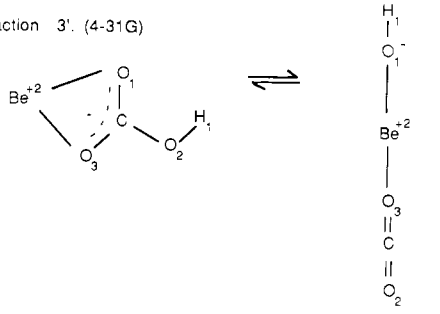

$\angle Q_1CH_1 = 30$

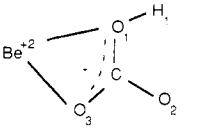

Reaction 4'. (PRDDO)

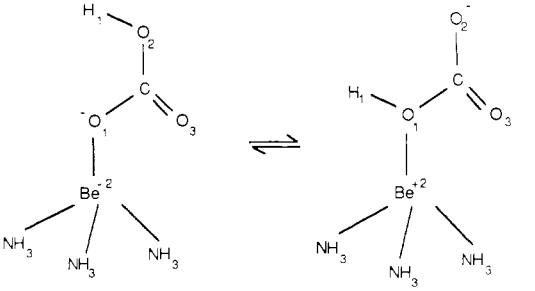

Reaction 2a. (PRDDO)

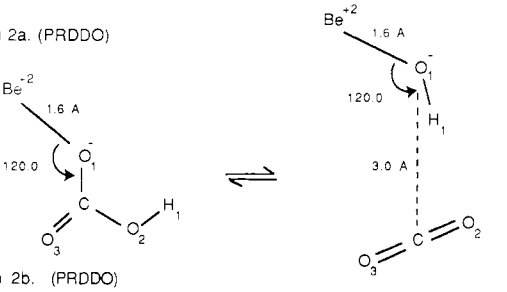

Reaction 2b. (PRDDO)

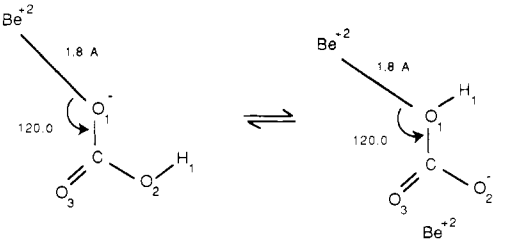

Reaction 2c. (PRDDO)

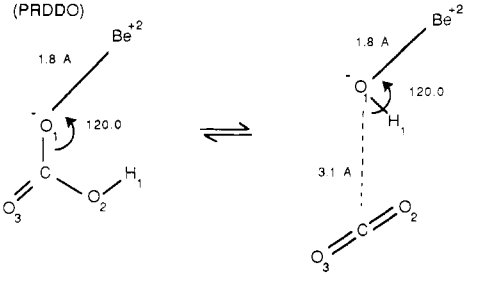

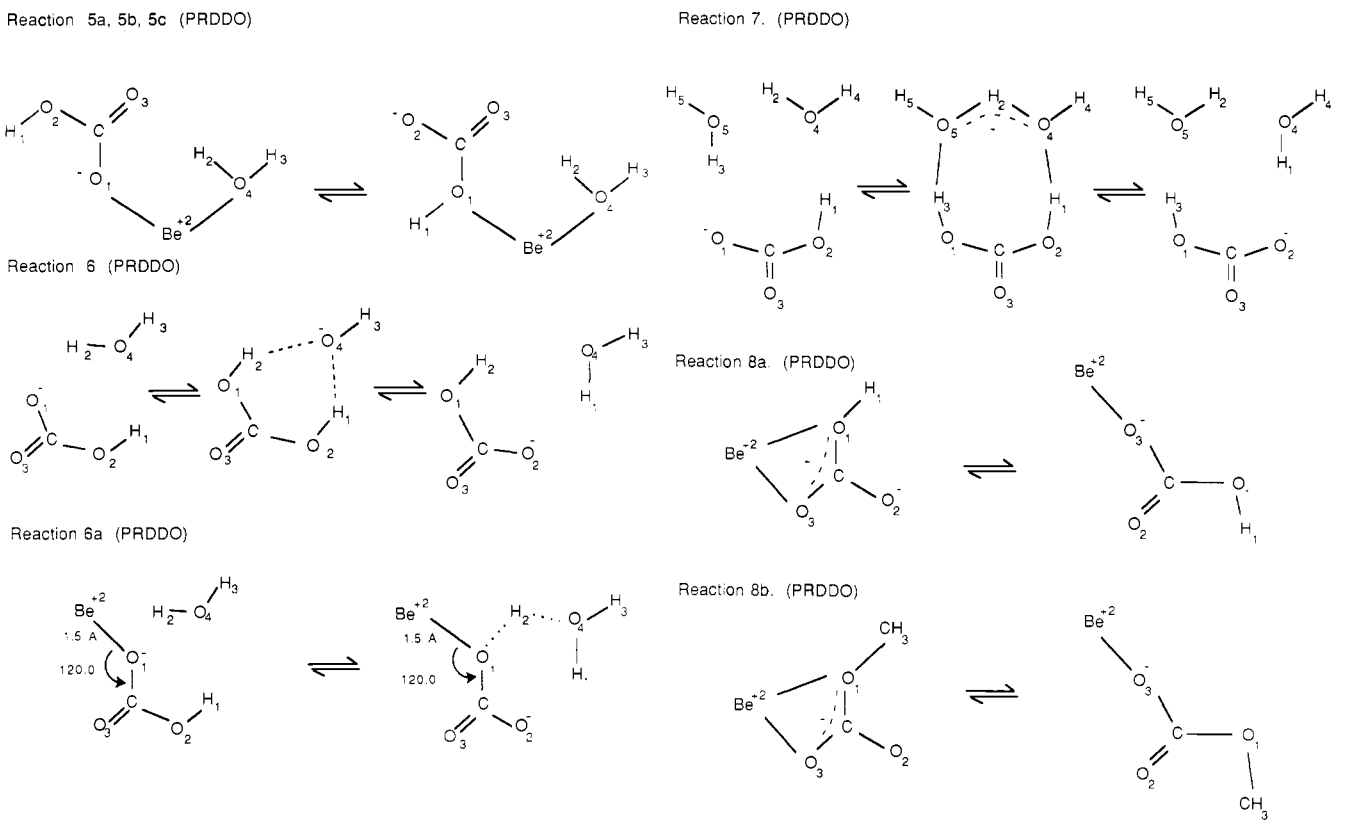

FIGURE 2: Reaction pathways of internal proton transfer of HCO_3^- studied under various catalytic conditions. The negative charge (−1) in the HCO_3^- molecule and the positive charge (+2) on zinc are marked symbolically. These charges are actually delocalized. Reaction 1: unfacilitated gas-phase reaction. Reaction 2: Zn^{2+} binds to O_1 of HCO_3^-. Reaction 3: Zn^{2+} binds to both O_1 and O_3 of HCO_3^-. Reactions 4 and 4a: in reaction 4, $Zn^{2+}(NH_3)_3$ binds to O_1 of HCO_3^-, with N–Zn–N = 109.47°, Zn–N = 2.021 Å, N–H = 1.025 Å, and H–N–Zn = 112.8°; in reaction 4a N–Zn–N optimizes to 95.6° and Zn–N = 2.02 Å, N–H = 1.025 Å, and H–N–Zn = 112.9°. Reaction 2′: Be^{2+} binds to O_1 of HCO_3^-. Reaction 3′: Be^{2+} binds to both O_1 and O_3 of HCO_3^-. Reaction 4′: $Be^{2+}(NH_3)_3$ binds to O_1 of HCO_3^-, with N–Be–N = 109.49°, Be–N = 1.76 Å, N–H = 1.03 Å, and H–N–Zn = 104.2°. Reactions 2b, 2c, and 2d: in reaction 2b, $Be–O_1$ = 1.6 Å, $Be–O_1–C$ = 120°, and the dihedral angle of $Be–O_1–C–O_3$ = 0.0°; the corresponding parameters for reaction 2c are 1.8 Å, 120°, and 0.0°, and for reaction 2d, 1.8 Å, 120°, and 180.0°. Reactions 5a, 5b, and 5c: Be^{2+} coordinates to O_1 of HCO_3^- with one water ligand on Be^{2+}; the $O_1–Be–O_4$ angle is 80°, 100°, and 120° for reactions 5a, 5b, and 5c, respectively. Reaction 6: one-water proton relay. Reaction 6a: Be^{2+} binds to O_1 of HCO_3^- in the one-water proton relay, where $Be–O_1$ = 1.5 Å and $Be–O_1–C$ = 120.0°. Reaction 7: two-water proton relay. Reaction 8a: reorientation of HCO_3^- relative to Be^{2+}. This reaction is the second half of the OH^--transfer mechanism proposed by Lindskog, as shown in Figure 3. Reaction 8b: reorientation of $CH_3CO_3^-$ relative to Be^{2+}.

the active site of carbonic anhydrase (Figure 2). The coordination of $(NH_3)_3$ to Zn^{2+} results in the transfer of 0.8 electrons from $(NH_3)_3$ to the $Zn^{2+}(HCO_3^-)$ complex. This not only neutralizes partially the positive charges on Zn^{2+} but also reduces electron withdrawal from HCO_3^- to Zn^{2+}; there is 0.4 electron withdrawn from HCO_3^- to Zn^{2+} in reaction 4, as compared with the normal 0.9 electron in reactions 2 and 3. Thus, reaction 4 leaves more electrons on HCO_3^- to stabilize the proton transfer. The barriers of reaction 4, with N–Zn–O = 109.47°, are 66.5 and 52.4 kcal/mol for the forward and the reverse reactions, respectively. When the N–Zn–O angle optimizes to 95.6° in reaction 4a (Figure 2), the barriers are 56.6 and 37.6 kcal/mol (Table II). The reaction paths of reactions 4 and 4a are similar.

Reactions 2′, 3′, and 4′. When Zn^{2+} of reactions 2, 3, and 4 is replaced by Be^{2+}, the corresponding reactions are 2′, 3′, and 4′ (Figure 2). In reactions 2′, 3′, and 4′, the $Be–O_1$ bond lengths are shorter than the corresponding $Zn–O_1$ bond lengths in reactions 2, 3, and 4 (Table I). Be^{2+} withdraws more electrons from HCO_3^- than Zn^{2+} at these shorter $Be–O_1$ bond lengths. The Mulliken charge on the beryllium ion of reaction 3′ is 0.86 electron, while that on the zinc ion of reaction 3 is 1.10 electrons. Despite the major differences between bond lengths of $Be–O_1$ and $Zn–O_1$ and between Mulliken charges on the beryllium ion and on the zinc ion, the electrostatic interactions between the positive charges on the beryllium ion and those on the transferring proton in reactions 3′ and 4′ are found to be similar to the corresponding electrostatic interactions between the positive charges on the zinc ion and those on the transferring proton in reactions 3 and 4. For instance, at the transition state of reaction 3, with Zn–H = 3.09 Å and the Mulliken charges of 1.106 on the zinc ion and 0.358 on the proton, the electrostatic repulsion is calculated to be 42.5 kcal/mol. This value compares with the corresponding interaction of 42.2 kcal/mol obtained at the transition state of reaction 3′, where Be–H = 2.74 Å and the Mulliken charges on the beryllium ion and on the proton are 0.868 and 0.402, respectively. This similarity of electrostatic effects in zinc-containing and beryllium-containing reactions may serve as the basis for deriving comparable reaction paths and energy barriers in reactions 3 and 3′ and in reactions 4 and 4′ (Tables I and II). Differences, however, exist between the paths of reactions 2 and 2′. Unlike reaction 2, $C–O_1$ is cleaved in the forward direction of reaction 2′. The product in PRDDO is a weakly bonded complex of $Be^{2+}(OH^-)$ and CO_2 (reaction 2′ (PRDDO), Figure 2).

In the 4-31G SCF MO studies of reactions 2′ and 3′, cleavage of $C–O_1$ occurs during the forward proton transfer. In the product, CO_2 and OH^- bind linearly to opposite sides of Be^{2+} (reactions 2′ and 3′ (4-31G), Figure 2). This linear conformation is unlikely to exist in the active site of carbonic anhydrase due to the presence of three imidazole ligands of

Table II: Energy Barriers

reaction	energy barrier[a] (kcal/mol) PRDDO	4-31G	4-31G+	4-31G**	4-31G**/MP2	6-31G**[b]
			Forward Reactions			
1	36.1	41.2	43.4	35.4	22.7	34.0
2	30.5					
2′	60.9	30.8	30.2	29.1	15.1	
2a	66.8					
2b	71.3					
2c	73.1					
3	67.5					
3′	66.3	72.6	72.3	71.4	53.5	
4	66.5					
4a	56.6					
4′	63.1					
5a	52.6 ± 1					
5b	50.7 ± 2					
5c	66.3 ± 4					
6	5.2	10.4	7.6	10.5	12.0	
6a	18.7					
7	1.4					
			Reverse Reactions			
1	36.1	41.2	43.4	35.4	22.7	34.0
2	69.4					
2′	36.7	117.1 (23.3)	117.3	109.9 (23.5)	96.5 (20.1)	
2a	44.3					
2b	40.3					
2c	72.0					
3	59.6					
3′	66.4	129.3 (51.3)	131.8	103.9 (43.4)	89.2 (31.7)	
4	52.4					
4a	37.6					
4′	28.7					
5a	30.0 ± 5					
5b	22.4 ± 5					
5c	30.5 ± 3					
6	5.2	10.4	7.6	10.5	12.0	
6a	3.1					
7	1.4					

[a] The values in parentheses are energy barriers obtained with H–C–O_1 restricted to 30.0 in the product. Energy barriers at the 4-31G+, 4-31G**, and 4-31G**/MP2 levels are evaluated at the 4-31G optimized geometries. [b] Geometries are optimized at the 6-31G** level. See footnotes of Table I.

Zn^{2+}. By restricting the O_1CH_1 angle to 30° during the 4-31G optimization, we obtain the second product structure, which is similar to the product obtained in the PRDDO calculations. The energy barrier for the reverse reaction of 2′ in 4-31G is reduced significantly from the original 117.1 kcal/mol for the linear product to 23.3 kcal/mol for the second (nonlinear) product.

Reactions 2a, 2b, and 2c. In reactions 2a, 2b, and 2c (Figure 2), the dependence of the reaction path and energy barrier on the relative orientation between Be^{2+} and HCO_3^- is examined. In reaction 2a, with $Be–O_1$ = 1.6 Å, $Be–O_1–C$ = 120°, and the dihedral angle of $Be–O_1–C–O_3$ = 0.0°, $C–O_1$ is cleaved in the forward proton transfer. As the bond length of $Be–O_1$ is extended from 1.6 Å in reaction 2a to 1.8 Å in reaction 2b, the cleavage of $C–O_1$ is avoided. When the dihedral angle of $Be–O_1–C–O_3$ is changed from 0.0° in reaction 2b to 180.0° in reaction 2c, $C–O_1$ is again cleaved.

Reactions 5a, 5b, and 5c. In reactions 5a, 5b, and 5c, we consider the internal proton transfer of HCO_3^- in the presence of both Be^{2+} and the water ligand of Be^{2+} (Figure 2). The water molecule that simulates the possible fifth water ligand on Zn^{2+} in carbonic anhydrase is found to transfer 0.3 electron to Be^{2+}, in addition to the transfer of 0.9 electron from HCO_3^- to Be^{2+}. The net charge on the beryllium ion is approximately 0.8 electron. This value is similar to the 0.86 electron on the beryllium ion when two oxygen atoms of HCO_3^- are coordinated to Be^{2+} in reaction 3′. The geometry optimization of the $Be^{2+}(HCO_3^-)(H_2O)$ complex leads to a linear arrangement of HCO_3^-, Be^{2+}, and H_2O. This linear arrangement is unlikely to exist in the active site of carbonic anhydrase because of the protein ligands as mentioned above. Restrictions on the $O_1–Be–O_4$ angle to 80°, 100°, and 120° are applied to reactions 5a, 5b, and 5c, respectively. In the resulting internal proton transfers, hydrogen H_2 is found to move flexibly between O_4 of H_2O and O_3 of HCO_3^- at small or no energy barriers. Overall, the energy barriers of reactions 5a, 5b, and 5c are modulated largely by the preassigned $O_1–Be–O_4$ angle and partly by the position of the hydrogen H_2 (Table II).

Reactions 6 and 6a. In reaction 6 (Figure 2), we examine the one-water proton relay for the internal protron transfer of HCO_3^-. The process consists of two consecutive steps: (1) H_2 of H_2O adds to HCO_3^- and forms the $H_2CO_3–OH^-$ complex at the transition state and (2) H_1 of H_2CO_3 adds to OH^- and forms the $HCO_3^-–H_2O$ complex in the product. During the proton relay of reaction 6, changes in both molecular geometries and charge distributions are small compared with those of the other reactions. Small reaction barriers are thus obtained for reaction 6. They are 4.98, 10.4, 7.6, and 10.5 kcal/mol in PRDDO, 4-31G, 4-31G+ and 4-31G**, respectively (Table II). Addition of Be^{2+} at O_1 with $Be–O_1–C$ = 120° and $Be–O_1$ = 1.5 Å yields reaction 6a. The forward barrier of reaction 6a is raised, relative to that of reaction 6, to 18.7 kcal/mol, and the reverse barrier is lowered to 3.1 kcal/mol (Table II). In the product of reaction 6a, proton H_2 is between O_1 and O_4 with $O_1–H_2$ = 1.1880 Å and $O_4–H_2$ = 1.1316 Å (Figure 2). Complete transfer of H_2 from O_4 to O_1 takes place after the subsequent cleavage of $C–O_1$ and leaving of CO_2 in the dehydration reaction; this process requires no energy barrier.

Reaction 7. In reaction 7, two-water proton relay is considered. The reaction barrier is small: 1.4 kcal/mol in PRDDO. At the transition state, H_3 of the first water molecule joins with HCO_3^- to form the H_2CO_3 molecule, and H_2 of the second water molecule is at equal distance with O_4 and O_5, bridging between the two hydroxide ions (Figure 2).

Discussion

The PRDDO method is used for most of the reactions studied in this paper. Although systematic errors are found in the PRDDO calculations, the qualitative properties are preserved (Halgren et al., 1978). For instance, in the nucleophilic attack of OH^- on the carbonyl carbon of FCHO to give $FCH_2O_2^-$, the well depths are 20 kcal/mol at OH^- to C of 2.01 Å with PRDDO and 17 kcal/mol at 2.25 Å with the 4-31G SCF MO method (Scheiner et al., 1976). Also, in the study of the reaction path of CO_2 with H_2O to give H_2CO_3 (Liang & Lipscomb, 1986), the molecular geometries of reactants, transition state, and product obtained by the PRDDO method are similar to those obtained in the other calculations (Liang & Lipscomb, 1986; Jonsson et al., 1976, 1977, 1978). For reactions 1, 3′, and 6 studied here, PRDDO is shown to yield reaction paths and energy barriers consistent with those obtained in the 4-31G SCF MO calculations. In general, PRDDO calculations provide us with reasonable starting reaction paths, to which complex calculations can be introduced to obtain more accurate results.

It is noted that 4-31G and PRDDO yield similar bond angles and that 4-31G gives slightly shorter bond lengths than PRDDO does (Table I). These results are consistent with Pople's finding that 4-31G gives shorter bond lengths than

STO-3G for small neutral molecules (Pople, 1977) [PRDDO is known to simulate efficiently the STO-3G SCF results (Ditchfield et al., 1971)]. 4-31G, in contrast, predicts longer bond lengths for hydrogen bonds, for bonds that involve Be^{2+}, and for bonds that are partially broken. This stabilizing effect of 4-31G for weak bonding at large bond distances probably originates from the double-ζ nature of the basis set. Unlike 4-31G, PRDDO with minimal basis is known to exaggerate the difficulties of bond cleavages (Scheiner et al., 1976). Although for most cases studied here 4-31G and PRDDO predict similar reaction paths, this difference between 4-31G and PRDDO in stabilizing fractional bonds may account for the dramatic discrepancy in the predicted reaction paths for reaction 3′: 4-31G requires that $C–O_1$ be cleaved, while PRDDO requires that $C–O_1$ remain bonded in the forward proton transfer (see Results).

Addition of diffuse orbitals on the heavy atoms in the 4-31G basis, yielding the 4-31G+ basis, lowers the energies of the positively and negatively charged molecules by approximately 20 and 6 kcal/mol, respectively. These stabilizing effects cancel in the evaluations of energy barriers, and the 4-31G+ calculations give barriers similar to those of the 4-31G calculations. Inclusion of polarization functions in the 4-31G basis and correction of correlation energies at the MP2 level, when evaluated at the 4-31G optimized geometries also lower the energy barriers (Table II). The qualitative properties are, nevertheless, preserved. In the study of the proton transfer in $H_3O_2^-$ (Szczesniak & Scheiner, 1982), $H_5O_2^-$ (Scheiner, 1981), and $NH_4^+H_2O$ (Scheiner, 1982), 4-31G calculations are shown to reproduce the barriers obtained from calculations including extended basis set and correlation energies. Nevertheless, no general conclusion that the 4-31G basis is adequate can be drawn.

In previous 4-31G studies, the energy barriers of internal proton transfer of formic acid, vinyl alcohol, and propene are calculated to be 59.5, 82.9, and 107.7 kcal/mol, respectively (Rodwell et al., 1980). Addition of polarization functions and electron correlations to these calculations are shown to systematically lower the barriers by ~15 kcal/mol. The internal proton transfer of formic acid is similar to the internal proton transfer of the bicarbonate ion studied here. The latter, however, has a smaller energy barrier (41.2 kcal/mol, Table II), probably due to the extra negative charges on HCO_3^-.

In reactions 2a, 2b, and 2c, different orientations of Be^{2+} relative to HCO_3^- are shown to lead to different reaction paths with different energy barriers (see Results). This implies that the particular orientation with which enzyme and substrate associate may be important in determining the specific enzymic reaction path. It is also noted that the presence of Be^{2+} and the restriction of the $Be–O_1–C$ angle to 120° in reaction 6a introduce more unfavorable interactions to product than to the other states (see Results). This effect largely accounts for the small energy barrier, 3.1 kcal/mol, for the reverse of reaction 6a and also illustrates one of the catalytic functions of enzymes in binding substrate loosely.

As illustrated under Results, the use of Be^{2+} to simulate the effects of Zn^{2+} is almost generally valid. In reaction 2′, which develops linear bonds about Be^{2+}, the unexpected cleavage of $C–O_1$ during forward proton transfer, although a specific failure of Be^{2+} to simulate the results of Zn^{2+} in reaction 2, provides us with a different pathway when a small electron population is found in the $C–O_1$ bond. Recently refined X-ray data of HCA II (Eriksson et al., 1986) have shown that water ligand and three imidazole ligands of Zn^{2+} are close to a tetrahedral geometry and that the distances between the three imidazole ligands and Zn^{2+} are very close to the 2.02 Å used here in reaction 4. Thus, for HCA II, cleavage of $C–O_1$ during internal proton transfer is unlikely to occur, especially when a one- or two-water proton relay is operating.

Among reactions studied here, the amount of forward proton transfer at the transition state exhibits the following ordering: reaction 4 > reaction 1 > reaction 3 > reaction 2. This ordering correlates with the bond strength of $O_1–H_1$ and also with the amount of positive charges on the zinc ion. The presence of Zn^{2+} or $Zn^{2+}(NH_3)_3$ is shown to raise the barriers of the internal proton transfer, primarily due to electron withdrawal from HCO_3^- to the zinc ion. The addition of one water ligand to Be^{2+} (reactions 5a, 5b, and 5c) lowers the reverse energy barrier. In reactions 6 and 7, inclusion of one or two water molecules as proton relay is shown to reduce the strain at the transition state and to introduce a certain amount of negative charge into the six- or eight-membered proton-transfer rings (Tables A and B, supplementary material). These stabilizing effects lead to the reduction of the energy barrier of proton transfer from 35.6 kcal/mol in the unfacilitated reaction (reaction 1) to 3.5 kcal/mol when one-water proton relay is included (reaction 6) and to 1.4 kcal/mol when two-water proton relay is included (reaction 7). In the hydration of CO_2 (Nguyen & Ha, 1984), H_2CO (Williams et al., 1983), and H_2C_2NH (Nguyen & Hegarty, 1983), similar stabilization of 26–46 kcal/mol is obtained when one extra water molecule is incorporated to relay the proton while the OH group of the first water is attacking nucleophilically at the electrophilic carbon. For carbonic anhydrase, there are two probable sources for the proton relay: the OH group of Thr-199, which is shown to be hydrogen bonded to the hydroxide group on zinc (Eriksson et al., 1986), and the solvent water molecules. The presence of solvent water in the active site of carbonic anhydrase is, therefore, catalytically important, both in relaying the proton in the internal proton transfer of HCO_3^- and in forming a water network for the proton transfer from Zn^{2+}-bound H_2O to His-64 (the proton-transfer group) in the deprotonation step. There is no equivalent water facilitation for the transfer of the alkyl group, R, in RCO_3^-. The barrier for alkyl transfer in RCO_3^- is normally much higher than that for the internal proton transfer of HCO_3^-. The barrier of CH_3 transfer in $CH_3CO_3^-$ is evaluated here to be 90.4 kcal/mol (PRDDO). Thus, the difficulty of alkyl-group transfer in alkyl carbonates may account for the absence of substrate activity of alkyl carbonates in carbonic anhydrase catalyzed reactions (Pocker & Deits, 1983).

In the remainder of this discussion we consider the role of the internal proton transfer in carbonic anhydrase catalyzed $CO_2–HCO_3^-$ exchange (reaction E). Reaction E is written

$$(EOH^-) + CO_2 \underset{k_{-1}}{\overset{k_1}{\rightleftharpoons}} (EOH^-)–CO_2 \underset{k_{-2}}{\overset{k_2}{\rightleftharpoons}} E–HCO_3^- \underset{k_{-3}}{\overset{H_2O\ k_3}{\rightleftharpoons}} EH_2O + HCO_3^- \quad \text{... (E)}$$

according to Lindskog's notation, in which step k_1 is equivalent to step 1 in Figure 1, step k_2 includes both steps 2 and 3, and step k_3 is modified step 4. The rate of $CO_2–HCO_3^-$ exchange in chemical equilibrium has been measured by observing the broadening of the ^{13}C NMR signals in the presence of carbonic anhydrase (Simonsson et al., 1979, 1982). The initial kinetic analysis of reaction E in HCA II indicates that k_{-2} and k_{-1} are the two probable rate-limiting steps (Simonsson et al., 1982). The subsequent study of the ^{13}C kinetic isotope effect in HCO_3^- dehydration (Paneth & O'Leary, 1985) further selects the k_{-2} step to be the rate-determining step. Step k_{-2} consists of the internal proton transfer (the reverse reaction

Table III: Geometry and Energy Parameters[a] for Reactions 8a and 8b as the Second Part of the OH^--Transfer Mechanism Proposed by Lindskog

	species in reaction 8a[b]			species in reaction 8b[b]		
	b	ts	c	b	ts	c
SCF energy	−34.5	0.0	−12.2	−33.0	0.0	−10.5
$C-O_1$	1.3453	1.3913	1.3908	1.3812	1.3743	1.3794
$C-O_2$	1.5013	1.3752	1.3676	1.4605	1.3927	1.3571
$C-O_3$	1.1785	1.2022	1.2075	1.2042	1.2016	1.2076
$Be-O_1$	1.5339	1.3651	1.3127	1.5379	1.3657	1.3124
$Be-O_1-C$	90.1	125.0	176.9	86.0	125.0	175.8
O_1-C-O_2	97.5	105.5	107.0	100.2	100.7	108.8
O_2-C-O_3	122.9	129.4	130.9	123.0	130.3	129.5

[a] Energies are in kcal/mol and bond lengths in angstroms. [b] Reaction 8a involves OH^- transfer and reaction 8b OCH_3^- transfer (Figure 3).

of step 3 in Figure 1) and the chemical dehydration step (the reverse reaction of step 2 in Figure 1), of which the internal proton transfer may contribute to the kinetic deuterium isotope effect. In fact, no isotope effect is detected (Simonsson et al., 1979, 1982). This result implies either that the rate-limiting step is not internal proton transfer, but HCO_3^- dehydration, or that if the internal proton transfer is rate limiting its transition-state structure should be highly unsymmetrical and thus would yield only negligible isotope effects (Jencks, 1969; More O'Ferrall, 1975). Our calculations have shown that the energy barrier of the internal proton transfer is small (1.4 kcal/mol; see Results) in the presence of the proton relay. This low barrier eliminates the possibility that the internal proton transfer is rate limiting. The HCO_3^- dehydration of k_{-2} is thus established to be the rate-limiting step in CO_2–HCO_3^- exchange.

The internal proton transfer in k_{-2} may take place either concertedly with or separately from the HCO_3^- dehydration, as the dehydration process determines the overall transition state. The reaction paths obtained in this paper favor separation of internal proton transfer from HCO_3^- dehydration. The independence of the rate of CO_2–HCO_3^- exchange of the buffer concentration (Simonsson, 1979, 1982) implies that no buffer molecules are involved in the proton relay during the internal proton transfer of Zn^{2+}-bound HCO_3^-.

To explain the absence of an isotope effect in CO_2–HCO_3^- exchange (reaction E), Lindskog (Lindskog et al., 1984) has proposed earlier for step k_{-2} the mechanism involving relocation of the OH^- moiety of the Zn^{2+}-bound HCO_3^-, in which the OH group is not on zinc, to a bidentate intermediate and then to Zn^{2+}-bound OH^- and CO_2, as shown in Figure 3. This mechanism does not involve any direct proton transfer, and thus no deuterium isotope effects are expected. According to earlier calculations (Pullman, 1981) the initial nucleophilic attack of Zn^{2+}-bound OH^- or CO_2 requires no activation energy. The subsequent reorientation of HCO_3^- relative to Be^{2+}, as studied here in reaction 8a (Figure 2), requires a barrier of 34.5 kcal/mol (Table III). As mentioned in our introduction, Pocker and Deit's experimental results (Pocker & Deits, 1983) show that alkyl carbonates, RCO_3^-, have no substrate activity in carbonic anhydrase catalyzed reactions. For Lindskog's OH^--transfer mechanism to be compatible with Pocker and Deit's results, it is necessary to show that OR^- transfer in RCO_3^- is nearly impossible. A barrier of 33 kcal/mol (Table III) obtained here for the CH_3O^- transfer in $CH_3CO_3^-$ (reaction 8b, Figure 2), is similar to that of OH^- transfer in HCO_3^- (reaction 8a). The reverse energy barriers for reactions 8a and 8b are 12.2 and 10.5 kcal/mol, respectively. Furthermore, the reaction paths and molecular structures along the paths for these two reactions are also similar (Table III). These results indicate that differences in reaction paths and energy barriers between CH_3O^- transfer

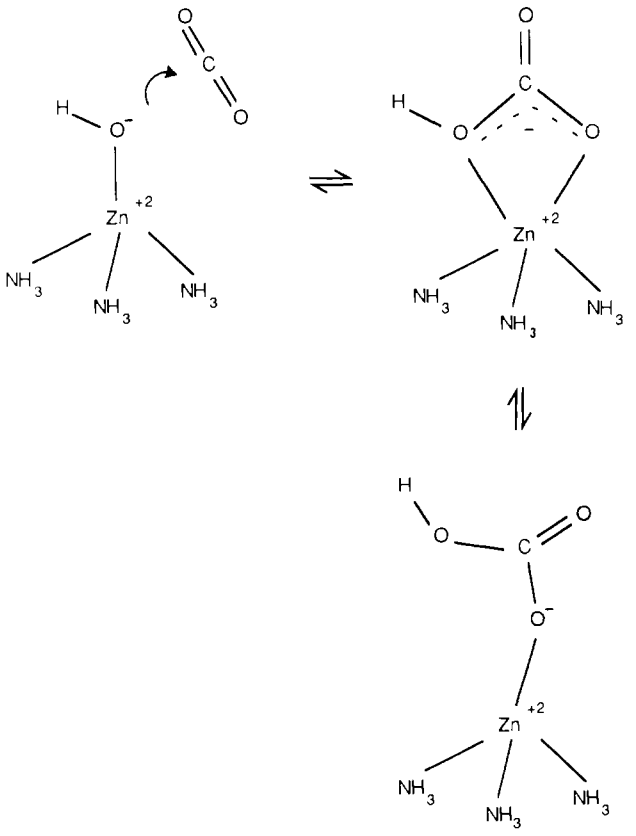

FIGURE 3: Relocation of the OH^- moiety during CO_2–HCO_3^- exchange from the Zn^{2+}-bound OH^- to the Zn^{2+}-bound HCO_3^-, with the OH group not on zinc. This mechanism is proposed by Lindskog (Lindskog et al., 1984) to account for the absence of a deuterium kinetic isotope effect in CO_2–HCO_3^- exchange. Note that the NH_3 molecules used here simulate the three imidazole ligands of Zn^{2+} from His-94, His-96, and His-119.

in $CH_3CO_3^-$ and OH^- transfer in HCO_3^- are insignificant and do not suffice to account for the absence of substrate activity of $CH_3CO_3^-$ in carbonic anhydrase catalyzed reactions. Substantial probable differences between these two reactions (reactions 8a and 8b) are steric hindrance and the rearrangement of water structure in the active site of carbonic anhydrase. Further investigations are required to resolve the effects.

This comparison of the OH^--transfer mechanism with internal proton transfer leads, in our view, to preference for the latter mechanism for conversion between two conformations of Zn^{2+}-bound HCO_3^- (step 3 of Figure 1) in carbonic anhydrase catalyzed reactions. The reasons are twofold. First, the energy barrier of the internal proton transfer is much lower than that of the OH^- transfer when appropriate proton relay is included in the proton transfer. Second, the mechanism of

internal proton transfer accounts successfully for the experimental results of Pocker and Diets, while the mechanism of OH^- transfer does not.

Supplementary Material Available

Mulliken's population analysis of atomic charge and bond order for PRDDO (Table A) and 4-31G (Table B) (4 pages). Ordering information is given on any current masthead page.

Registry No. HCA II, 9001-03-0; HCO_3^-, 71-52-3; CO_2, 124-38-9; Zn, 7440-66-6; Be, 7440-41-7.

References

Clark, T., Chandrasekhar, J., Spitznagel, G. W., & von Ragué Schleyer, P. (1983) *J. Comput. Chem. 4*, 294.

Coleman, J. E., et al. (1980) in *Biophysics and Physiology of Carbon Dioxide* (Bauer, C., Gros, G., & Bartels, H., Eds.) pp 133–285, Springer-Verlag, Berlin.

Ditchfield, R., Hehre, W. J., & Pople, J. A. (1971) *J. Chem. Phys. 54*, 724.

Eriksson, E. A., Jones, T. A., & Liljas, A. (1986) in *Zinc Enzymes* (Bertini, I., Luchinat, C., Maret, W., & Zeppezauer, M., Eds.) pp 317–328, Birkhauser, Boston.

Fersht, A. (1977) in *Enzyme Structure and Mechanism*, p 69, Freeman, San Francisco.

Halgren, T. A., & Lipscomb, W. N. (1973) *J. Chem. Phys. 58*, 1569.

Halgren, T. A., Kleier, D. A., Hall, J. H., Jr., Brown, L. D., & Lipscomb, W. N. (1978) *J. Am. Chem. Soc. 100*, 6595.

Hariharan, P. C., & Pople, J. A. (1973) *Theor. Chim. Acta 28*, 213.

Jencks, W. P. (1969) in *Catalysis in Chemistry and Enzymology*, pp 259–273, McGraw-Hill, New York.

Jönsson, B., Karlström, G., & Wennerström, H. (1976) *Chem. Phys. Lett. 41*, 317.

Jönsson, B., Karlström, G., Wennerström, H., Forsén, S., Roos, B., & Almlof, J. (1977) *J. Am. Chem. Soc. 99*, 4628.

Jönsson, B., Karlström, G., & Wennerström, H. (1978) *J. Am. Chem. Soc. 100*, 1658.

Liang J.-Y., & Lipscomb, W. N. (1986) *J. Am. Chem. Soc. 108*, 5051.

Lindskog, S. (1983) in *Zinc Enzymes* (Spiro, T. G., Ed.) p 77, Wiley, New York.

Lindskog, S., Engberg, P., Forsman, C., Ibrahim, S. A., Jonsson, B.-H., Simonsson, I., & Tibell, L. (1984) *Ann. N.Y. Acad. Sci. 429*, 61.

Lipscomb, W. N. (1983) *Annu. Rev. Biochem. 52*, 17.

Marynick, D. S., & Lipscomb, W. N. (1982) *Proc. Natl. Acad. Sci. U.S.A. 79*, 1341.

Møller, C., & Plesset, M. S. (1934) *Phys. Rev. 46*, 618.

More O'Ferrall, R. A. (1975) in *Proton-Transfer Reaction* (Caldin, E., & Gold, V., Eds.) pp 201–263, Wiley, New York.

Mulliken, R. S. (1955) *J. Chem. Phys. 23*, 1833.

Nguyen, M. T., & Hegarty, A. F. (1983) *J. Am. Chem. Soc. 105*, 3811.

Nguyen, M. T., & Ha, T. K. (1984) *J. Am. Chem. Soc. 106*, 599.

Paneth, P., & O'Leary, M. H. (1985) *J. Am. Chem. Soc. 107*, 7381.

Pocker, Y., & Sarkanen, S. (1978) *Adv. Enzymol. Relat. Areas Mol. Biol. 47*, 149.

Pocker, Y., & Deits, T. L. (1983) *J. Am. Chem. Soc. 105*, 980.

Pople, J. A. (1977) in *Applications of Electronic Structure Theory* (Schaefer, H. F., III, Ed.) pp 1–24, Plenum, New York.

Prince, R. H. (1979) *Adv. Inorg. Chem. Radiochem. 22*, 349.

Pullman, A. (1981) *Ann. N.Y. Acad. Sci. 367*, 340.

Pullman, A., & Demoulin, D. (1979) *Int. J. Quantum Chem. 16*, 641.

Rodwell, W. R., Bouma, W. J., & Radom, L. (1980) *Int. J. Quantum Chem. 18*, 107.

Scheiner, S. (1981) *J. Am. Chem. Soc. 103*, 315.

Scheiner, S. (1982) *J. Phys. Chem. 86*, 376.

Scheiner, S., Lipscomb, W. N., & Kleier, D. A. (1976) *J. Am. Chem. Soc. 98*, 4770.

Simonsson, I., Jonsson, B. H., & Lindskog, S. (1979) *Eur. J. Biochem. 93*, 409.

Simonsson, I., Jonsson, B. H., & Lindskog, S. (1982) *Eur. J. Biochem. 129*, 165.

Szczešniak, M. M., & Scheiner, S. (1982) *J. Chem. Phys. 77*, 4586.

Williams, I. H., Spangler, D., Femec, D. A., Maggiorn, G. M., & Schowen, R. L. (1983) *J. Am. Chem. Soc. 105*, 31.